

## THE DISTRIBUTION OF QUIET SUN MAGNETIC FIELD STRENGTHS FROM 0 TO 1800 G

I. DOMÍNGUEZ CERDEÑA

Instituto de Astrofísica de Canarias, E-38205 La Laguna, Spain

J. SÁNCHEZ ALMEIDA

Instituto de Astrofísica de Canarias, E-38205 La Laguna, Spain

AND

F. KNEER

Institut für Astrophysik, Friedrich-Hund-Platz 1, D-37077 Göttingen, Germany

## ABSTRACT

The quiet Sun photospheric plasma has a variety of magnetic field strengths going from zero to 1800 G. The empirical characterization of these field strengths requires a probability density function (PDF), i.e., a function  $P(B)$  describing the fraction of quiet Sun occupied by each field strength  $B$ . We show how to combine magnetic field strength measurements based on the Zeeman effect and the Hanle effect to estimate an unbiased  $P(B)$ . The application of the method to real observations renders a set of possible PDFs, which outline the general characteristics of the quiet Sun magnetic fields. Their most probable field strength differs from zero. The magnetic energy density is a significant fraction of the kinetic energy of the granular motions at the base of the photosphere (larger than 15% or larger than  $2 \times 10^3$  erg cm<sup>-3</sup>). The unsigned flux density (or mean magnetic field strength) has to be between 130 G and 190 G. A significant part of the unsigned flux (between 10 % and 50 %) and of the magnetic energy (between 45 % and 85 %) are provided by the field strengths larger than 500 G which, however, occupy only a small fraction of the surface (between 1% and 10%). The fraction of kG fields in the quiet Sun is even smaller, but they are important for a number of reasons. The kG fields still trace a significant fraction of the total magnetic energy, they reach the high photosphere, and they appear in unpolarized light images. The quiet Sun photosphere has far more unsigned magnetic flux and magnetic energy than the active regions and the network all together.

*Subject headings:* Sun: fundamental parameters – Sun: magnetic fields – Sun: photosphere

## 1. INTRODUCTION

The interior of the supergranulation cells does not seem to be magnetic according to the standard full disk magnetograms. Livingston & Harvey (1975) and Smithson (1975) improved the standard sensitivity to discovered weak magnetic signals in the cell interiors. These elusive signals are known as Inter-Network fields (IN), Intra-Network fields or, simply, quiet Sun fields. Characterizing these quiet Sun fields is important since they may play a role in the physics responsible for the global solar magnetism (Unno 1959; Stenflo 1982; Yi et al. 1993; Sánchez Almeida 1998, 2004; Schrijver & Title 2003). The quiet Sun could easily contain most of the photospheric unsigned magnetic flux and magnetic energy, simply because it occupies most of the solar surface (more than 90 %, even at solar maximum; Harvey-Angle 1993).

Our understanding of the quiet Sun magnetic fields has improved during the last years thanks to advances in instrumentation (e.g. Grossmann-Doerth et al. 1996; Sánchez Almeida et al. 1996; Sigwarth et al. 1999; Lin & Rimmele 1999; Lites 2002; Domínguez Cerdeña et al. 2003a,b; Khomenko et al. 2003; Sánchez Almeida et al. 2004), diagnostic capabilities (e.g. Stenflo 1982; Faurobert-Scholl 1993; Faurobert-Scholl et al. 1995; Landi Degl’Innocenti 1998; Sánchez Almeida & Lites 2000; Socas-Navarro & Sánchez Almeida 2002;

Trujillo Bueno et al. 2004; Manso Sainz et al. 2004; Sánchez Almeida 2005), as well as numerical simulations (e.g. Cattaneo 1999; Emonet & Cattaneo 2001; Stein & Nordlund 2002; Vögler 2003; Vögler et al. 2005). The new spectropolarimeters make it possible to detect the low polarimetric signals characteristic of the IN fields. Sophisticated diagnostic techniques are needed to interpret those signals, which depend in a non-trivial way on the (a priori unknown) physical properties of the magnetized plasma. For example, opposite polarities often coexist in the resolution elements giving rise to very asymmetric line profiles requiring special methods of diagnostic (see, e.g., Sánchez Almeida & Lites 2000; Lites 2002). The numerical simulations provide guidance for the magnetic field topology to be expected, a knowledge critical for a proper interpretation of the observables.

The magnetic field strength is one of the key parameters to characterize the magnetism of the quiet Sun. Its study has a rather long tradition, with a period of unsuccessful attempts (Unno 1959; Howard & Bhatnagar 1969; Stenflo & Lindgren 1977), followed by the first estimates by Stenflo (1982) and Faurobert-Scholl (1993) based on Hanle depolarization measurements. The observed Hanle signals agree with a volume-filling mixed-polarity magnetic field of constant field strength (Stenflo 1982; Faurobert-Scholl 1993; Faurobert-Scholl et al. 1995; Faurobert et al. 2001; Stenflo et al. 1997). The value of the estimated mean field strength has increased upon refinement of the diagnostic techniques. The most recent estimate by Trujillo Bueno et al. (2004) and Bommier et al. (2005) are consistent with a

Electronic address: itahiza@iac.es

Electronic address: jos@iac.es

Electronic address: kneer@astro.physik.uni-goettingen.de

constant field of 60 G (or a mean field of 130 G assuming an exponential distribution of magnetic field strengths). Most measurements of the quiet Sun magnetic fields are based on interpreting line polarization signals caused by the more familiar Zeeman effect. They show a rather different magnetism, with structures occupying a small fraction of the solar surface and having intense fields in the range of the hectogauss (hG) and the kilogauss (kG). Actually, the field strength depends in a systematic way on the Zeeman splitting of the spectral line employed to measure. The works using visible lines deduce the presence of kG magnetic fields (Grossmann-Doerth et al. 1996; Sánchez Almeida & Lites 2000; Socas-Navarro & Sánchez Almeida 2002; Domínguez Cerdeña et al. 2003a,b), while measurements based on infrared (IR) lines infer sub-kG field strengths (Lin & Rimmele 1999; Khomenko et al. 2003). This apparent inconsistency among the various measurements of field strength, plus the guidance of numerical simulations of magneto-convection, suggest that the quiet Sun has a continuous distribution of field strengths going all the way from 0 G to 2 kG (Sánchez Almeida & Lites 2000; Socas-Navarro & Sánchez Almeida 2003; Trujillo Bueno et al. 2004). Therefore, each one of the individual measurements mentioned above is biased, providing only a partial view of the magnetic fields existing in the quiet Sun. We think that this biased information can be cleaned up and assembled to provide a reasonable estimate of the intrinsic magnetic field strength distribution. This work describes a method to recover such information.

Due to the variety of field strengths, they are best characterized by a probability density function PDF. The magnetic field strength PDF,  $P(B)$ , is defined as the probability that a point of the atmosphere chosen at random has a magnetic field strength  $B$ . Alternatively, it describes the fraction of quiet Sun occupied by fields with a strength  $B$ . The PDF approach to characterizing the quiet Sun field strength is both convenient and powerful. First, one can directly compare observations with numerical simulations, which predict  $P(B)$ . Second, it concentrates basic information on the quiet Sun magnetism, e.g., the first moment  $\langle B \rangle$  is connected with the unsigned magnetic flux density<sup>1</sup>, whereas the second moment provides the magnetic energy density  $\langle B^2 \rangle / (8\pi)$ ,

$$\langle B \rangle = \int_0^\infty B P(B) dB, \quad (1)$$

$$\langle B^2 \rangle = \int_0^\infty B^2 P(B) dB. \quad (2)$$

There are several observational magnetic field strengths PDFs in the literature (see the references cited in the previous paragraph). As we pointed out above, all of them are known to be severely biased. On the one hand, those based on Hanle signals miss the strong fields, since the Hanle depolarization does not vary for field strengths above a threshold that is typically smaller than a few hundred G (see, e.g., Landi Degl'Innocenti 1992; Stenflo 1994; Trujillo Bueno 2001). On the other hand, the Zeeman measurements show only a small fraction

of the existing magnetic structures (see, e.g., Stenflo 1982; Sánchez Almeida et al. 2003). The Zeeman signals tend to cancel when opposite polarities coexist in the resolution elements. We detect only the residuals left when the cancellation is not perfect (e.g., when the two polarities do not have exactly the same magnetic flux, when strong Doppler shifts separate the absorption produced by the two polarities, when the temperature imbalance between polarities creates net signals, and so on). Here we try to get rid of all these observational biases to produce an empirical  $P(B)$ . We approach the problem by assuming a flexible yet reasonable shape for the expected PDF. This guess is based on recent numerical simulations of magneto-convection, as well as on the latest Hanle and Zeeman observations. The actual  $P(B)$  is set by forcing the PDF to meet several observational and theoretical constraints. So far as we are aware of, this is the first quiet Sun PDF satisfying magnetic field strength observations going all the way from 0 G to 2 kG. (The premises were already put forward by Sánchez Almeida 2004, though.) The success of the trial is only partial since rather than a single PDF we derive a family compatible with the present observations. However, the approach is shown to be viable, so that future more precise observations will allow us to narrow down the range of possibilities.

The paper is organized as follows; § 2 describes how to piece together all the ingredients needed to estimate an unbiased PDF. Some of the more tedious details are completed in Appendix A. The properties of the PDFs satisfying the observational constraints are extracted and analyzed in § 3. In particular, we compare the semi-empirical PDFs with theoretical PDFs coming from numerical simulations of magneto-convection. Finally, § 4 summarizes the main conclusions, discusses their consequences, and points out the natural way to proceed.

## 2. SYNTHESIS OF THE PDF

In order to facilitate the reading of this detailed section, we start off by listing the thread of the argument.

1. The *unbiased* quiet Sun PDF can be approximated by a linear combination of the *biased* PDFs inferred from Zeeman signals and from Hanle signals (§ 2.1).
2. The shape of the Zeeman PDF is obtained from observations. The shape of the Hanle PDF is not constrained by observations, and so we take it from numerical simulations of magneto-convection (§ 2.1).
3. The Hanle and Zeeman signals come from different photospheric heights. One needs a transformation to express them in a common height, in other words, a recipe for the variation with height in the atmosphere of the PDFs (§ 2.2).
4. Piecing together this information, we work out a semi-analytical PDF depending on three free parameters. One needs only three independent observables to set it (§ 2.3).

### 2.1. The shape of the PDF

The Zeeman induced polarization changes the sign depending on the orientation of the vector magnetic field with respect to the observer. When magnetic fields with varied directions coexist in the resolution elements, the net polarization tends to cancel. The lack of polarization is interpreted

<sup>1</sup> Strictly speaking, the unsigned magnetic flux density across a plane is given by the average of the unsigned component of the magnetic field in the direction perpendicular to the plane. Consequently, we are not precise when using the term *unsigned magnetic flux density* for  $\langle B \rangle$ , which is the average of the magnetic field vector modulus. There is no possible misunderstanding, though. The term is employed consistently throughout the text, and the actual unsigned flux is never mentioned except in this footnote.

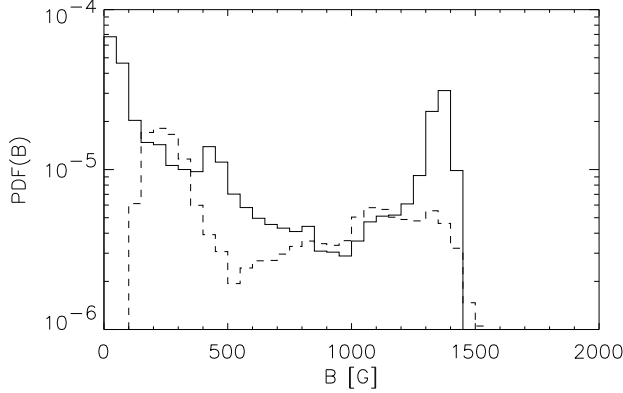


FIG. 1.— PDFs inferred from Zeeman signals of Fe I  $\lambda 6301.5$  Å, Fe I  $\lambda 6302.5$  Å, Fe I  $\lambda 15648$  Å, and Fe I  $\lambda 15652$  Å observed simultaneously in a quiet Sun region. The two PDFs come from the same data set. The solid line represents a MISMA inversion (Domínguez Cerdeña et al. 2005) whereas the dashed line corresponds to a Milne-Eddington inversion (Sánchez Almeida et al. 2003). The MISMA PDF is shown some 100 km above the base of the photosphere, at a height corresponding to the Milne-Eddington inversion. The PDFs are normalized to the fraction of quiet Sun producing Zeeman polarization signals ( $\sim 1.5\%$ ).

as absence of magnetic fields, so that the Zeeman measurements underestimate the volume occupied by magnetic fields. This bias increases with decreasing field strength, since the Zeeman signals scale with the field strength. The Hanle induced depolarization does not suffer the cancellation of the Zeeman signals. However, the Hanle induced depolarization is insensitive to magnetic field strengths larger than a few hundred G (e.g., Landi Degl’Innocenti 1992; Stenflo 1994; Trujillo Bueno 2001; Sánchez Almeida 2005). Thus the biases of the Hanle and Zeeman measurements turn out to be complementary. Keeping in mind this complementarity, one can approximate the true unbiased PDF,  $P(B)$ , as a linear combination of the biased PDF inferred from Zeeman signals,  $P_Z(B)$ , plus the biased PDF that fits the Hanle signals,  $P_H(B)$ ,

$$P(B) = w P_H(B) + (1 - w) P_Z(B), \quad (3)$$

with  $P_H(B)$  and  $P_Z(B)$  normalized to unity, and the weight  $w \simeq 1$ . A full derivation of this equation is given in Appendix A.

Regarding  $P_Z(B)$ , we take the shape of the biased PDF measured by Domínguez Cerdeña et al. (2005). It is based on a realistic semi-empirical modeling of 2280 Stokes profiles of Fe I  $\lambda 6301.5$  Å, Fe I  $\lambda 6302.5$  Å, Fe I  $\lambda 15648$  Å, and Fe I  $\lambda 15652$  Å observed simultaneously in a quiet Sun region. These four spectral lines are complementary since those in the visible spectral range sense preferentially the kG fields whereas the IR lines tend to detect hG field strengths (Sánchez Almeida & Lites 2000; Socas-Navarro & Sánchez Almeida 2002, 2003). The empirical Zeeman PDF shape adopted here is not very different from the one derived by means of Milne-Eddington fits to the same Stokes profiles (see Sánchez Almeida et al. 2003; Domínguez Cerdeña 2004). The two PDFs are shown in Figure 1. Both are rather broad with a local maximum at kG fields. The differences are unimportant for the present work, and they are discussed in detail by Domínguez Cerdeña et al. (2005).

The Hanle effect modifies the polarization produced in scattering processes, and so it only affects lines formed in NLTE

(non-local thermodynamic equilibrium). Hanle based studies are therefore restricted to lines formed high in the atmosphere, where the collisions are low enough for the scattering events to be frequent. However, we need Hanle signals formed as low as possible, so that they can be compared with Zeeman signals produced in the low-mid photosphere. The Hanle signals of Sr I  $\lambda 4607$  Å are formed particularly low (e.g. Faurobert-Scholl et al. 1995). In addition, this line allows a simple treatment of the usually very complex synthesis of the Hanle signals (see, Faurobert et al. 2001, and also the discussion in § 2.3). Sr I  $\lambda 4607$  Å is chosen to constrain the PDF for these two unusual properties. As it is argued in, e.g., Sánchez Almeida (2005), the Hanle signals of Sr I  $\lambda 4607$  Å do not constrain the shape of the PDF. This limitation is overcome here by parameterizing the shape of  $P_H(B)$  using an analytic function. The Hanle signals have been interpreted with approximations using Dirac  $\delta$ -functions, exponential functions, and Maxwellian distributions (e.g., Stenflo 1982; Faurobert-Scholl 1993; Trujillo Bueno et al. 2004; Sánchez Almeida 2004), but these shapes do not fit in our needs. First, we expect a continuous distribution of field strengths, which discards Dirac  $\delta$ -functions. Second, the exponential fall off with field strength,

$$P_H(B) = \frac{1}{\langle B \rangle} \exp(-B/\langle B \rangle), \quad (4)$$

is too pronounced according to the PDFs resulting from numerical simulations of magneto-convection (see, e.g., the dotted line in Figure 2a). The Maxwellian distribution can be discarded with the same argument, since the fall off is even more pronounced than the exponential one. Inspired by the numerical simulations of magneto-convection developed with the MuRAM code (Vögler 2003; Vögler et al. 2005), we choose a log-normal distribution  $P_H(B)$ ,

$$P_H(B) = \frac{1}{\sqrt{\pi}\sigma B} \exp[-(\ln B - \ln B_0)^2/\sigma^2], \quad (5)$$

with  $B_0$  and  $\sigma$  two parameters related to the two first moments of the distribution,

$$\langle B \rangle = B_0 \exp(\sigma^2/4), \quad (6)$$

and

$$\langle B^2 \rangle = B_0^2 \exp(\sigma^2). \quad (7)$$

Figure 2 compares numerical PDFs from Vögler (2003) with fits using log-normal functions and exponential functions. (All the fits were performed for  $B < 500$  G.) The two plots correspond to an initial vertical field of 10 G (Figure 2a) and 50 G (Figure 2b), and the parameters of the log-normal PDFs are  $\sigma = 2.5$ ,  $B_0 = 5$  G, and  $\sigma = 1.7$ ,  $B_0 = 38$  G, respectively. The log-normal fits are much better than the exponentials, and we choose them to represent  $P_H(B)$ . A comment is in order. The log-normals tend to zero when  $B \rightarrow 0$  G. Actually, they reach a maximum at  $B = B_{\max}$  with,

$$B_{\max} = B_0 \exp(-\sigma^2/2). \quad (8)$$

Counterintuitive as it sounds, the property of having a maximum is to be expected for the true quiet Sun PDF. When the field strength is small enough, the magnetic fields are easily modified and randomized by the convective motions. Those weak fields are expected to have an isotropic distribution of field directions, with the three components of the magnetic field being independent. Suppose that the magnetic field

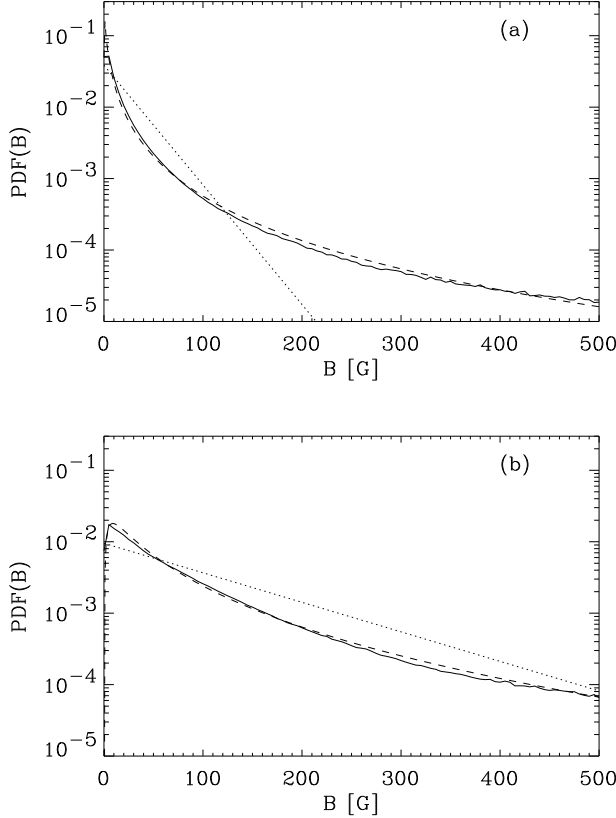


FIG. 2.— Fits of quiet Sun PDFs from numerical simulations of magneto-convection (the solid lines; Vögler 2003) using log-normal functions (the dashed lines) and exponential functions (the dotted lines). The log-normals are far superior. The upper and lower panels differ in the initial field strength of the simulation; 10 G (a) and 50 G (b), respectively. The PDFs correspond to the base of the photosphere.

strength of these weak fields has a typical value  $B_i$  different from zero but otherwise arbitrary. For a point of the atmosphere to have  $B = 0$  the three components of the magnetic field vector must be zero simultaneously. This event is highly improbable since the three components are independent. Consequently, it is to be expected that  $P(B) \rightarrow 0$  when  $B \ll B_i$ . The drop at small fields is also clearly seen in some numerical simulations of magneto-convection (e.g., Figure 2b; Figure 3 in Cattaneo 1999; Figure 5.25 in Vögler 2003).

## 2.2. Vertical variation of the PDF

The photosphere is strongly stratified, with the gas pressure decreasing exponentially with the height in the atmosphere. Part of the pressure that maintains the mechanical balance of a magnetic structure is provided by the magnetic pressure, which has to decrease to keep up with the pressure drop. Since the magnetic flux is conserved, the decrease of field strength comes together with an expansion of the field lines and an increase of the volume occupied by the magnetic fields (see, e.g., Spruit 1981a). These two effects modify the PDF. As we pointed out above, the Hanle signals are formed high in the photosphere. In order to use them to constrain a PDF at the base of the photosphere, one needs to know how the PDF varies with height. Working out such variation is a non trivial problem, closely connected with the so-called extrapolation of the photospheric fields to the chromosphere and

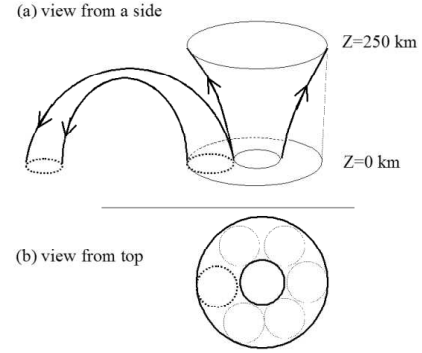


FIG. 3.— (a) Cartoon with two magnetic fluxtubes. The field lines of one of them reach the mid photosphere ( $z = 250$  km). The field lines of the second one bend over and return below this photospheric height. (b) A view from the top of the first fluxtube. The thick solid circles outline the sections of the fluxtube at  $z = 0$  km (small circle) and  $z = 250$  km (large circle). Note that for the fluxtube to expand a number of other concentrations around it cannot reach  $z = 250$  km. The section of those that must return are represented by dotted circles in the cartoon.

corona (e.g., Sakurai 1989; Schrijver & Title 2003). Here we develop a crude approximation, which suffices for the kind of exploratory investigation carried out in the paper but which, eventually, will require further refinement.

We start off by introducing a new symbol for the PDF at a height in the atmosphere  $z$ ,  $\wp(B, z)$ , so that the PDF discussed so far corresponds to the base of the photosphere<sup>2</sup>,

$$P(B) = \wp(B, 0). \quad (9)$$

Our estimate is based in the so-called thin fluxtube approximation (e.g., Spruit 1981a,b). In this approximation, the magnetic field strength of an isolated static structure surrounded by field free plasma drops with the height in the atmosphere as the square root of the field free gas pressure. In our case,

$$B(z) \simeq B(0) \exp(-z/H_B), \quad (10)$$

with magnetic field strength scale height  $H_B$  twice the gas pressure scale height, and so, independent of the field strength. The cross-section of one of these thin fluxtubes  $S$  increases with height as the field strength decreases. The need to conserve the magnetic flux imposes,

$$S(B(z), z) = S(B(0), 0) \exp(z/H_B), \quad (11)$$

so that the product  $BS$  does not depend on  $z$ . The expansion is made at the expense of the field free plasma surrounding the magnetic concentration. In our case there is no such field free plasma, so that an increase of the volume occupied by one magnetic structure requires shrinking the volume occupied by others (see the two magnetic concentrations in Figure 3a). Which physical parameter determines why some concentrations expand whereas others shrink? The magnetic forces responsible for the expansion or contraction scale with the square of the magnetic field strength. Then it is to be expected that the expansion of the strongest fields prevails, making it

<sup>2</sup> The height  $z = 0$  corresponds to the base of the photosphere in the one-dimensional mean quiet Sun model atmospheres (e.g. Maltby et al. 1986), where the continuum optical depth  $\tau_c = 1$  and the total pressure is  $\simeq 1.2 \times 10^5$  dyn cm<sup>-2</sup>.

difficult for the weak fields to reach high photospheric layers. We use this idea as an ansatz to proceed. For a magnetic concentration to expand from  $S(B(0), 0)$  to  $S(B(z), z)$ , its field strength has to be the largest in the area  $S(B(z), z)$  around it (see Figure 3b). If in average all magnetic concentrations have the same section, then a concentration will survive if and only if it has the largest field strength among the  $n - 1$  concentrations around it, with

$$n \simeq \frac{S(B(z), z)}{S(B(0), 0)}; \quad (12)$$

see Figure 3b. The probability that one concentration has a field strength smaller than  $B$  at  $z = 0$  is,

$$M(B) = \int_0^B P(B') dB'. \quad (13)$$

Since the field strengths of different concentrations are independent, the probability that  $n - 1$  have fields smaller than  $B$  is  $M(B)^{n-1}$  and, consequently, a magnetic field strength  $B$  reaches  $z$  with a probability,

$$F_P(B) = M(B)^{n-1}. \quad (14)$$

This probability of survival  $F_P(B)$  allows us to write down the PDF at  $z$ , namely,

$$\wp(B(z), z) dB(z) = \frac{S(B(z), z)}{S(B(0), 0)} F_P(B(0)) \wp(B(0), 0) dB(0), \quad (15)$$

where we have taken into account that the atmosphere occupied for those magnetic fields that survive increases as  $S(B(z), z)/S(B(0), 0)$ . Using equations (9), (10), (11), and (12), one can rewrite equation (15) in a compact way,

$$\wp(B, z) = n^2 P(nB) \left[ \int_0^{nB} P(B') dB' \right]^{n-1}. \quad (16)$$

It is not difficult to show that  $\wp(B, z)$  is properly normalized even for non-integer  $n$ , which we interpret as a sign of self consistency in the derivation of equation (16).

Equation (16) provides the PDF at any height given  $n$  and the PDF at height equals zero. We apply such recipe to the Hanle signals of Sr I  $\lambda 4607$  Å when they are formed as close as possible to the disk center (i.e., as low as possible in the photosphere). This lowest height of formation turns out to be about 250 km (Faurobert-Scholl et al. 1995). On the other hand, a  $H_B \simeq 230$  km is obtained from the stratification of  $B$  in the inversions performed by Domínguez Cerdeña et al. (2005), which renders,

$$n = \exp(250 \text{ km}/H_B) \simeq 3. \quad (17)$$

Figure 4 shows the variation with height predicted by equation (16) for an exponential  $P(B)$  (a), and a log-normal  $P(B)$  (b). One can compare the original PDFs (the dashed lines) with the PDFs at  $z = 250$  km (the solid lines). Note how the maximum of  $P(B)$  is shifted to stronger fields as one moves up in the photosphere. This is to be expected since the probability of survival of weak fields is very low.

### 2.3. Physical constraints

Once  $P_Z(B)$  has been set according to the prescription in § 2.1, The analytical PDF in equation (3) depends on three free parameters; the weight  $w$ , and the two parameters  $\sigma$  and  $B_0$  defining the shape of the Hanle PDF (equation [5]). They

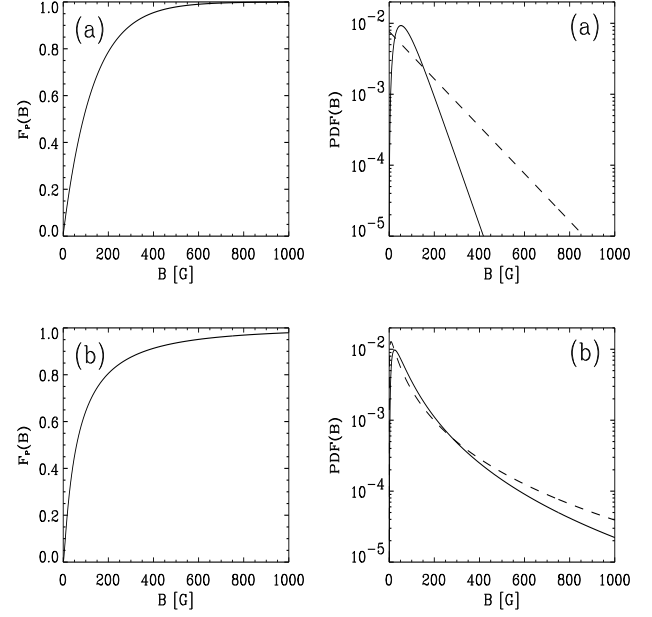


FIG. 4.— Examples of the change with height in the photosphere of an exponential PDF (a) and a log-normal PDF (b). The plots in the first column show the probability of survival  $F_P(B)$ . The plots in the second column represent the PDF at  $z = 0$  (the dashed lines), and the PDF at  $z = 250$  km (the solid lines). (The PDFs correspond to those shown in Figure 2b.)

can be set using three *independent* observables. Unfortunately, only one observable plus one lower limit are available. First, the fraction of the photosphere producing the observed Zeeman signals is a few per cent (e.g. Lin & Rimmele 1999; Sánchez Almeida & Lites 2000; Domínguez Cerdeña et al. 2003a; Lites & Socas-Navarro 2004). This fraction represents a lower limit to the true percentage of quiet Sun with strong fields, which constrains  $1 - w$  (equation [A17]). In particular, the signals used to estimate  $P_Z(B)$  arise from some 1.5 % of the surface (Domínguez Cerdeña et al. 2005). Taking this value as our lower limit,  $1 - w > 1.5 \times 10^{-2}$ , and so,

$$w < 0.985. \quad (18)$$

Second, the Hanle depolarization signals of Sr I  $\lambda 4607$  Å,  $Q/Q_0$ , depend on the PDF approximately as,

$$Q/Q_0 = \int_0^\infty \wp(B, z) W_B(B) dB, \quad (19)$$

with the kernel  $W_B(B)$  given by,

$$W_B(B) = 1 - \frac{2}{5} \left( \frac{\gamma_H^2}{1 + \gamma_H^2} + \frac{4\gamma_H^2}{1 + 4\gamma_H^2} \right), \quad (20)$$

$$\gamma_H = \frac{B}{50 \text{ G}};$$

see, Faurobert et al. (2001), Sánchez Almeida (2005), and references therein. Using equations (16) and (17), equation (19) can be rewritten as,

$$Q/Q_0 \simeq 9 \int_0^\infty W_B(B) P(3B) \left[ \int_0^{3B} P(B') dB' \right]^2 dB. \quad (21)$$

The work by Trujillo Bueno et al. (2004) gives our best estimate of  $Q/Q_0$ ,

$$Q/Q_0 = 0.41 \pm 0.04, \quad (22)$$

with the error bars representing the standard deviation among different observations made at a fixed heliocentric angle. Fulfilling equations (21) and (22) warrants producing the observed Sr I  $\lambda 4607$  Å Hanle depolarization. We will refer to them as the *Hanle constraint*.

Lacking of additional observables to determine a single  $P(B)$ , we resort to a general consideration of theoretical nature. The magnetic energy associated with the quiet Sun magnetic fields has to be smaller than the kinetic energy of the granular motions, otherwise the non-magnetic numerical simulations of solar granulation would not be so successful in reproducing all kinds of observables (see Stein & Nordlund 1998; Asplund et al. 2000). In other words,

$$\chi \ll 1, \quad (23)$$

if  $\chi$  is the ratio between the magnetic energy and the kinetic energy of the granular motions at the base of the photosphere,

$$\frac{\langle B^2 \rangle}{8\pi} = \chi \frac{1}{2} \langle \rho u^2 \rangle. \quad (24)$$

Using the typical convective velocities  $u$  and densities  $\rho$  at  $z = 0$  km ( $\rho \simeq 3 \times 10^{-7}$  g cm $^{-3}$ ,  $u \simeq 3$  km s $^{-1}$ ; Stein & Nordlund 1998, Figure 5), one gets a kinetic energy density of some  $1.3 \times 10^4$  erg cm $^{-3}$ . This value allows us to rewrite equation (24) as,

$$\chi = \langle B^2 \rangle / (580 \text{ G})^2. \quad (25)$$

### 3. RESULTS

The PDF in equation (3) depends on three free parameters. As it is discussed in § 2.3, we do not have three independent constraints to determine a single  $P(B)$ . There is one genuine constraint (equations [21] and [22]) and two lower limits (equations [18] and [23]). This problem rules out selecting one PDF for the quiet Sun magnetic field strength. Instead, we are forced to explore the set of PDFs compatible with the observables, and then to distill properties common to all of them. The strategy of the search and the common properties are described next.

Given  $\sigma$ , we produce a grid of  $18 \times 30$   $P(B)$  with  $0.83 \leq w \leq 1$ , and  $5 \text{ G} \leq B_0 \leq 150 \text{ G}$ . It suffices to include all the possibilities allowed by the observational and theoretical constraints. For each PDF we compute the total magnetic energy in units of the kinetic energy ( $\chi$  in equation [25]), and the Sr I  $\lambda 4607$  Å Hanle signals to be expected (equation [21]). The magnetic energy and the Hanle signals as a function of  $w$  and  $B_0$  are shown in the plots of the first column of Figure 5 (column a). The total energy is represented by the solid contours. The dashed lines trace those pairs  $w - B_0$  compatible with the observed depolarization (22). The shaded strips around these dashed lines correspond to the error bars of the depolarization. The five plots portray four different values of  $\sigma$  (0.5, 1, 1.75, and 2.5), plus the case of exponential Hanle PDFs (equation [4]). The first column of Figure 5 shows that the magnetic energy is always important (say, larger than 15 % of the kinetic energy of the granular motions). This conclusion turns out to be independent of  $B_0$  and  $\sigma$  provided that  $w$  fulfills the limit (18).

The third column in Figure 5 shows specific PDFs for three pairs  $w - B_0$  producing the observed Hanle signals. The dashed line, the dotted line and the solid line correspond to the circle, the cross and the square in the first column, respectively. They differ mainly because of  $w$ , a parameter controlling the importance of the tail of strong fields, with little

influence on the core of the PDF at low field strengths. As we discuss in § 2.1, the PDFs present a maximum in this core of small  $B$ . (The most probable magnetic field strength differs from zero.) Since the Hanle constraint determines  $B_0$  almost independently of  $w$  (the dashed lines in Figures 5a are nearly horizontal), the position of this maximum is controlled by  $\sigma$  (see equation [8]). Figure 6 shows how the magnetic field strength of the maximum  $B_{\max}$  increases with decreasing  $\sigma$  to become  $B_{\max} \simeq 180 \text{ G}$  when  $\sigma \rightarrow 0$ . This limit can be explained keeping in mind that  $P(B)$  tends to a Dirac  $\delta$ -function  $\delta(B - B_0)$  when  $\sigma \rightarrow 0$  (see equation [5]). A Dirac  $\delta$ -function at  $B \simeq 60 \text{ G}$  accounts for the Hanle constraint (22) (Trujillo Bueno et al. 2004; Bommier et al. 2005; Sánchez Almeida 2005). According to the recipe that we use for the variation with height of the PDFs (equations [16] and [17]), a  $\delta(B - 60 \text{ G})$  at the height where Sr I  $\lambda 4607$  Å is formed corresponds to  $\delta(B - 180 \text{ G})$  at  $z = 0$ , which explains the limit  $B_{\max} \simeq 180 \text{ G}$ .

In order to illustrate some other details of the PDFs fulfilling the observational constraints, we select a representative one having a few additional desirable properties. It will be denoted as the *reference* PDF. In principle, there are no arguments to prefer a specific  $B_{\max}$ , and a wide range of values is compatible with the observables (Figure 6). However, we tend to think that small  $B_{\max}$  PDFs are more realistic, since they seem to be preferred by the numerical simulations of magneto-convection (Emonet & Cattaneo 2001; Stein & Nordlund 2002; Vögler 2003; Vögler et al. 2005). Small  $B_{\max}$  implies large  $\sigma$ , but  $\sigma$  cannot be arbitrarily large since the magnetic energy of the PDF increases with  $\sigma$  (Figure 5a), and the magnetic energy must comply with the limit (23). We choose  $\sigma = 1.75$ , which yields  $B_{\max} \simeq 13 \text{ G}$ . This selection together with  $w = 0.94$  leads to the reference PDF shown in Figure 7. It has an energy 28% of the kinetic energy ( $\chi = 0.28$ ), and an unsigned flux density  $\langle B \rangle \simeq 150 \text{ G}$ . The dashed line in Figure 7a also shows the reference PDF at 250 km, computed according to the recipe in equation (16). The latter has an unsigned flux density of 120 G, similar to the flux of the exponential PDF used by Trujillo Bueno et al. (2004) to account for the Hanle constraint in equation (22). The magnetic energy at  $z = 250 \text{ km}$  is three times smaller than the energy at the base of the photosphere. Figure 7b compares our reference PDF and simulated PDFs from Vögler (2003) with initial fields of 10 G (the dotted line), 50 G (the dashed line), and 200 G (the dotted-dashed line). These 3D simulations solve the MHD equations for a compressible partly ionized plasma. After a purely hydro-dynamic transient, an initial homogeneous and vertical field is introduced. The processing and amplification of these seed fields lead to additional magnetic flux, which amounts to 25 G, 100 G and 270 G, for the three different initial fields. The reference PDF turns out to be a mixture between the 200 G PDF ( $B < 600 \text{ G}$ ) and the 50 G PDF ( $1000 \text{ G} < B < 1500 \text{ G}$ ). Note that the two numerical PDFs have a small broad local maximum at large magnetic fields ( $B \sim 1500 \text{ G}$ ). Our semi-empirical PDF also has a maximum at large fields, except that it is more pronounced, and it occurs at higher fields ( $B \simeq 1700 \text{ G}$ ). The existence of such maximum at high field strengths can be understood as the result of a magnetic intensification process from weak to strong fields. The magnetic energy piles up at the largest possible field strength, set by the value whose magnetic pressure exceeds the gas pressure of a non-magnetic atmosphere in mechanical equilibrium ( $\sim 1800 \text{ G}$  at  $z = 0 \text{ km}$ ).

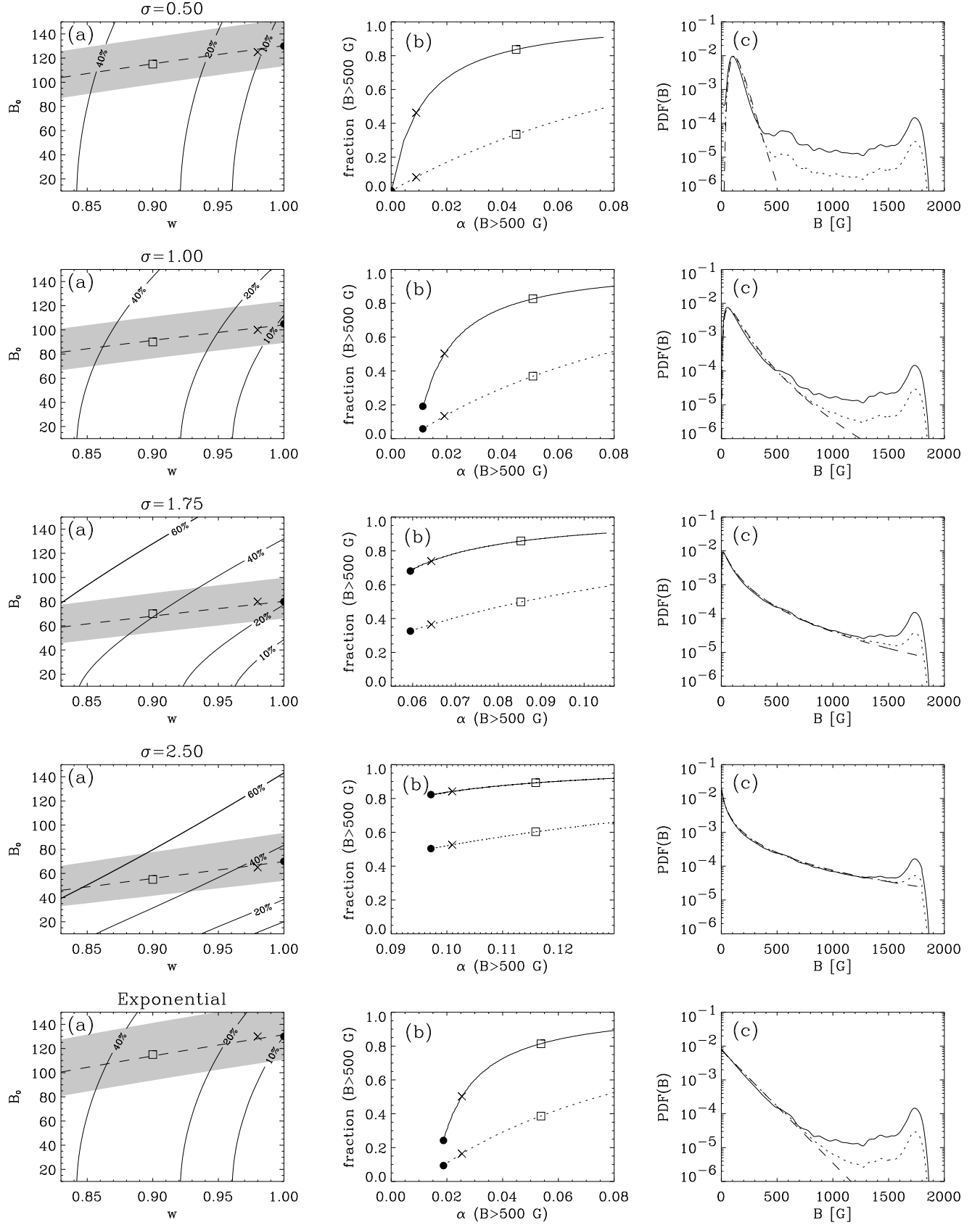


FIG. 5.— (a) Magnetic energy density of the PDFs as a function of the free parameters  $w$  and  $B_0$  (the solid contours). The labels give the magnetic energy in percent of the kinetic energy of the granular motions. The dashed lines show those pairs  $w - B_0$  fulfilling the Hanle constraint, with the shaded strips representing to the range of observed depolarizations. The different plots portray different values of the parameters  $\sigma$ , plus the case of an exponential Hanle PDF included for reference (bottom; in this case  $B_0 = \langle B \rangle$ ). The three symbols correspond to the three symbols in the second column, and to the three PDFs of the third column (see below). (b) Fraction of quiet Sun unsigned magnetic flux density (the dotted line) and of magnetic energy density (the solid line) in the form of strong fields ( $B > 500$  G). They are represented versus their filling factor  $\alpha(B > 500$  G). The curves correspond to pairs  $w - B_0$  fulfilling the Hanle constraint (the dashed lines of the first column). (c) PDFs corresponding to the three symbols in the first and the second columns. The solid line corresponds to the square ( $w = 0.9$ ), the dotted line to the times symbol ( $w = 0.98$ ), and the dashed line to the bullet ( $w = 1.0$ ).

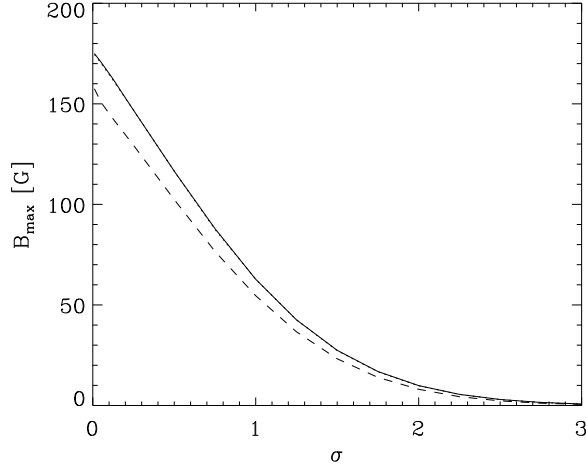


FIG. 6.— Magnetic field strength at which  $P(B)$  is maximum versus  $\sigma$ . The different curves have different  $w$ ; 1, 0.98 and 0.9, for the solid line, the (barely visible) dotted line, and the dashed line, respectively.

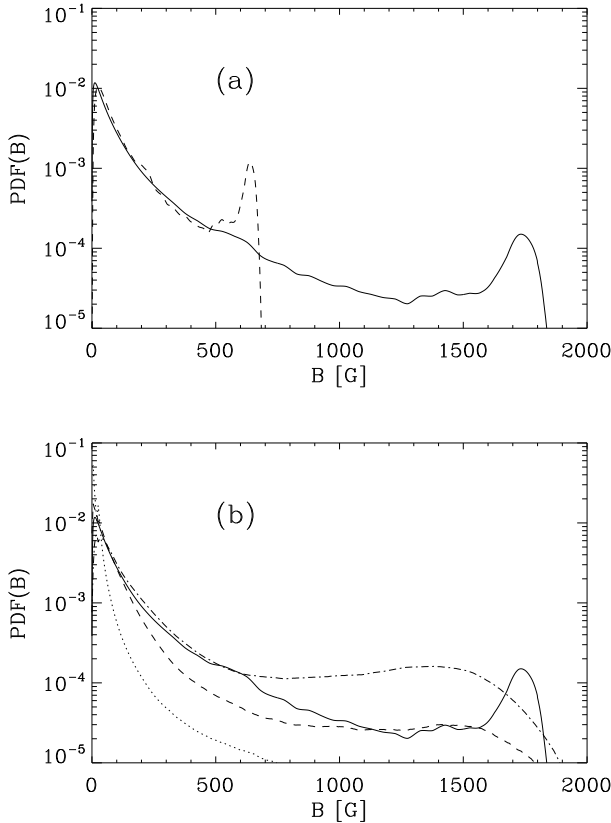


FIG. 7.— Reference PDF with  $\sigma = 1.75$  and  $w = 0.94$ . (a) PDF at  $z = 0$  km (the solid line) and at  $z = 250$  km (the dashed line). (b) Comparison of  $P(B)$  at  $z = 0$  (the solid line) with PDFs from numerical simulations of magnetoconvection by Vögler (2003) having initial field strengths of 10 G (the dotted line), 50 G (the dashed line) and 200 G (the dotted-dashed line).

(A detailed explanation of the mechanism can be found in Domínguez Cerdeña et al. 2005.)

We are particularly interested in understanding which part of the quiet Sun magnetism is provided by strong fields which,

among other things, are responsible for most of the observed Zeeman signals (see Appendix B), and can be studied in unpolarized light (see below). In order to quantify the contribution, we use the first moments of the PDF. Specifically, the fraction of quiet Sun occupied by strong fields,

$$\alpha(B > B^*) = \int_{B^*}^{\infty} P(B) dB, \quad (26)$$

the fraction of unsigned magnetic flux,

$$\phi(B > B^*) = \frac{1}{\langle B \rangle} \int_{B^*}^{\infty} B P(B) dB, \quad (27)$$

and fraction of magnetic energy,

$$\varepsilon(B > B^*) = \frac{1}{\langle B^2 \rangle} \int_{B^*}^{\infty} B^2 P(B) dB. \quad (28)$$

Choosing a somewhat arbitrary threshold between weak and strong fields<sup>3</sup>, we use

$$B^* = 500 \text{ G}, \quad (29)$$

for the plots in the second column (b) of Figure 5. They show the fraction of unsigned flux (the dotted line) and magnetic energy (the solid line) versus the volume occupied by the strong fields. Only PDFs producing the observed Hanle depolarization are considered (those corresponding to the dashed lines in the first column of Figure 5). The dots, crosses and squares also correspond to the dots, crosses and squares in the first column of Figure 5. In all cases with  $w < 0.98$  (indicated by the cross symbols), the fraction of magnetic energy in strong fields is larger than 50% (between 45% and 85% when  $0.5 \leq \sigma \leq 2.5$ ), although they fill only a small fraction of the surface (between 1% and 10%). The contribution is disproportionate. As far as the unsigned flux is concerned, the strong field still provide a sizeable fraction (between 10% and 50% for  $0.5 \leq \sigma \leq 2.5$ ). The reference PDF ( $\sigma = 1.75$ ,  $w = 0.94$ ) has 42 % of the unsigned flux in  $B > 500$  G, a figure similar to the estimates by Socas-Navarro & Sánchez Almeida (2003, 38%) and Sánchez Almeida (2004, 36%).

According to a physical mechanism originally proposed by Spruit (1976), the very strong fields are expected to be bright in unpolarized images. Part of the pressure required to maintain the plasma in mechanical balance is provided by the magnetic pressure. When the magnetic pressure of a particular structure is comparable to the mean gas pressure of the atmosphere, the structure must have low mass density and so it becomes transparent. We see deeper through the magnetized structure, and deeper often means hotter and brighter. The mean pressure at  $z = 0$  is equivalent to a magnetic pressure provided by a field strength of some 1800 G. In order to estimate which fraction of the quiet Sun magnetic fields could be bright, we consider the strongest magnetic fields in the PDFs, say, those larger than two-thirds of the maximum value, or larger than 1200 G. Figure 8a shows  $\alpha(B > B^*)$  versus  $B^*$  for three representative PDFs fulfilling the Hanle constraint. The reference PDF corresponds to the solid line. The filling factor in bright features is always very small, e.g.,  $\alpha(B > 1200 \text{ G}) = 2.5 \%$  in the reference PDF. Yet, these fields are responsible for 25 % of the unsigned flux and 50 % of the magnetic energy of the quiet

<sup>3</sup> This figure is not far from the value of a magnetic field strength yielding equipartition between magnetic energy density and kinetic energy density; see equation (25) with  $\chi = 1$ .



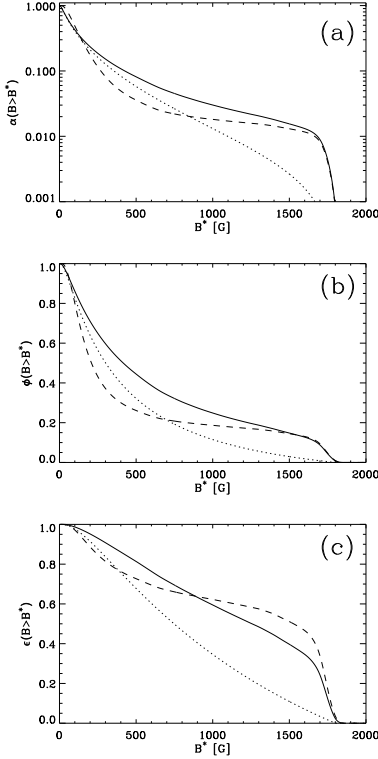


FIG. 8.— Filling factor (a), fraction of unsigned magnetic flux (b), and fraction of magnetic energy (c) in field strengths stronger than  $B^*$ . The three curves correspond to three PDFs fulfilling the Hanle constraint with  $\sigma = 1.75$  and  $w = 0.94$  (the solid line, and also the reference PDF),  $\sigma = 1.75$  and  $w = 1$  (the dotted line), and  $\sigma = 1$  and  $w = 0.94$  (the dashed line).

Sun magnetic fields. Sánchez Almeida et al. (2004) detected (G-band) bright points in the quiet Sun covering some 0.7 % of the supergranular cell interiors. Although the percentage is smaller than the surface coverage in strong fields mentioned above, the two figures may not necessarily disagree. As it is pointed out by Sánchez Almeida et al. (2004), the observed value is strongly biased and it represents a lower limit. Only the largest magnetic concentrations pop up above the dark intergranule background (Title & Berger 1996) and, moreover, not all kG are expected to be bright (Sánchez Almeida et al. 2001; Vögler 2003).

So far the value of  $Q/Q_0$  given in equation (22) has been used as the Hanle constraint. In order to explore the dependence of the results on  $Q/Q_0$ , we also tried  $Q/Q_0 \simeq 0.6$ , which is the Hanle depolarization inferred and used by Faurobert et al. (2001). The main effect is decreasing the value of  $B_0$  needed to reproduce the observations, and so, decreasing the magnetic field where  $P(B)$  is maximum ( $B_{\max}$ , see equation [8]). This shift of  $B_{\max}$  can be achieved without a large variation of the unsigned magnetic flux and magnetic energy. This is due to the fact that the tail of hG and kG field strengths is the mayor contributor to the flux and energy, and this tail is not very sensitive to  $B_0$ , and so, to  $B_{\max}$ . For instance, the reference PDF ( $w = 0.94$ ,  $\sigma = 1.75$ ) has  $B_{\max} = 3$  G,  $\langle B \rangle = 70$  G, and  $\chi \simeq 0.17$  when  $Q/Q_0 \simeq 0.6$ , whereas  $B_{\max} = 13$  G,  $\langle B \rangle = 150$  G, and  $\chi \simeq 0.28$  when  $Q/Q_0 \simeq 0.41$ . This moderate change in  $\langle B \rangle$  and  $\chi$  must be compared with the case where the tail of strong fields is not present ( $w = 1$  in equation [3]). Then  $\langle B \rangle \propto B_{\max}$  and  $\chi \propto B_{\max}^2$  (equations [6], [7], and [8]), which implies a very large decrease of the un-

signed flux (a factor of four) and energy (a factor of twenty) to fit a depolarization signal of  $Q/Q_0 \simeq 0.6$ .

The unsigned magnetic flux and magnetic energy assigned by our semi-empirical PDFs to the quiet Sun is far larger than the unsigned flux and energy in the form of active regions and the network, even at solar maximum. The reference PDF has  $\langle B \rangle \simeq 150$  G and  $\langle B^2 \rangle^{1/2} \simeq 305$  G. Consider the regular full disk magnetograms, which are mostly sensitive to the active regions and the network (see § 1). At solar maximum, these magnetograms show a total unsigned magnetic flux across the solar surface of some  $7 \times 10^{23}$  Mx (e.g., Harvey-Angle 1993, Chapter 12). Dividing this magnetic flux by the area of the solar surface, the unsigned flux density in the form of active regions and the network  $\langle B \rangle_{AR}$  turns out to be,

$$\langle B \rangle_{AR} \sim 12 \text{ G} \sim 0.08 \langle B \rangle, \quad (30)$$

where we have used for  $\langle B \rangle$  the unsigned flux of the reference PDF. If all these active region magnetic fields are intrinsically strong with  $B \sim 1500$  G, then

$$\langle B^2 \rangle_{AR} \simeq 1500 \text{ G} \langle B \rangle_{AR} \sim (135 \text{ G})^2 \sim 0.2 \langle B^2 \rangle. \quad (31)$$

#### 4. CONCLUSIONS

The quiet Sun magnetic fields may be central to understand the global magnetic properties of the Sun, but they are not well characterized from an empirical point of view. They present a variety of physical properties and so their description must be carried out in terms of probability density functions (PDFs). This work is focused on characterizing the PDF of the field strength, which describes the fraction of quiet Sun occupied by each field strength. We use the symbol  $P(B)$  for the PDF at the base of the photosphere<sup>4</sup>. The PDFs existing in the literature provide only a partial view – each individual measurement samples only a small range of field strengths (see § 1). Our paper proposes a semi-empirical  $P(B)$  that tries to get rid of all the biases and so, for the first time, it covers all the range of possible field strengths from  $B = 0$  G to  $B \simeq 1800$  G. It combines Hanle effect based measurements, Zeeman effect based measurements, and some general ansatzs inspired by numerical simulation of magneto-convection and the thin fluxtube approximation (§ 2). The procedure is of general nature and eventually, it will allow us to determine a single PDF characteristic of the quiet Sun magnetic fields. So far the observational and theoretical constraints only provide a range of PDFs. The constraints used in this work are: (a) reproducing the Hanle depolarization signals of Sr I  $\lambda 4607$  Å, (b) having a filling factor for strong fields larger than the filling factor inferred from the observed Zeeman signals, and (c) having a magnetic energy density smaller than the kinetic energy density of the granular motions.

The properties common to all  $P(B)$  fulfilling these constraints are analyzed in § 3. They provide a qualitative picture of the quiet Sun magnetic field plus some quantitative results.

- The magnetic energy density is a significant fraction of the kinetic energy density of the granular motions. Larger than some 15% of the kinetic energy at the base of the photosphere.
- Most of the surface is occupied by weak magnetic fields. We find that magnetic fields weaker than 500 G fill between 90% and 99% of the surface.

<sup>4</sup> Where the continuum optical depth at  $\lambda 5000$  Å is one, and the total pressure  $\simeq 1.2 \times 10^5$  dyn cm<sup>-2</sup>.

- The most probable field strength is not zero. This result has a novel consequence. The existence and position of such maximum is a direct indication of the presence of large amounts of unsigned magnetic flux in the quiet Sun. Its presence represents a specific prediction of the work, and it may be tested observing Hanle signals of lines with assorted sensitivities to weak magnetic fields.
- The magnetic energy tends to be concentrated in strong fields independently of the parameters chosen for the PDF. Between 45 % and 85 % of the energy is in the form of fields stronger than 500 G which occupy only a small fraction of the quiet Sun (between 1 % and 10 %). The unsigned magnetic flux of these strong fields represent between 10 % and 50 % of the quiet Sun unsigned flux. Since the strong fields reach the upper photosphere more easily than the weak ones (§ 2.2), they may be particularly influential in connection with the chromospheric and coronal magnetism (e.g. Schrijver & Title 2003).
- The tail of very strong kG fields of the PDFs is expected to be bright in high spatial resolution unpolarized images (Spruit 1976). Sánchez Almeida et al. (2004) detected (G-band) bright points in the quiet Sun supergranulation cell interiors covering some 0.7 % of the surface. The filling factors predicted here are larger but not necessarily incompatible. The observed bright points are only a fraction of the existing ones (the largest and brightest ones). Despite the minute fraction of the surface that it covers, this tail of kG fields contains a significant part of the quiet Sun magnetic energy. They have the practical advantage with respect to the weak fields of showing up in unpolarized light.
- The unsigned magnetic flux and magnetic energy assigned by our semi-empirical PDFs to the quiet Sun are far larger than the unsigned flux and energy in the form of active regions and the network, even at solar maximum.

The sensitivity of the current Zeeman measurements allows us to detect spatially resolved uniform magnetic fields of one G or even smaller (e.g., Keller et al. 1994; Lites et al. 1996; Lin & Rimmele 1999; Khomenko et al. 2003). Most of the solar surface is occupied by magnetic fields with strengths larger than this sensitivity limit which, however, do not show up in the measurements (c.f. the Zeeman inferred PDFs in Figure 1 with the reference PDF in Figure 7). The Zeeman signals seem to be dominated by the strong magnetic fields, despite the fact they only fill a small part of the solar surface. As we explain in Appendix B, the reason is twofold. First, the Zeeman signals are sensitive to the magnetic flux, and the unsigned magnetic flux in the form of weak and strong fields is comparable. Second, all Zeeman signals tend to cancel, but the cancellation of opposite polarity low field strength signals is more effective. Typically, there are many more weak mag-

netic field features per resolution element than strong magnetic field features. Then the weak fields cancel more often than the strong fields, and the latter are detected in a larger proportion. (See Appendix B for quantitative arguments.)

Our conclusions are in the vein of previous works assigning large amounts of unsigned magnetic flux and magnetic energy to the quiet Sun (Sánchez Almeida & Lites 2000; Domínguez Cerdeña et al. 2003a; Sánchez Almeida et al. 2003; Sánchez Almeida 2003; Sánchez Almeida 2004; Trujillo Bueno et al. 2004; Bommier et al. 2005). On the other hand, they seem to contradict another line of research indicating that the quiet Sun is not so magnetically active (Faurobert-Scholl 1993; Wang et al. 1995; Faurobert et al. 2001; Khomenko et al. 2005). As we discuss in § 1, all previous estimates are known to be biased, and so, they require model-dependent corrections to go from the actual measurements to the solar magnetic fluxes and energies. Possibly a significant part of the discrepancy can be pinned down to such corrections, and it will be cured upon refinement of the techniques and improvement of the statistical significance of the results.

A quiet Sun as magnetic as the one advocated here may pose a problem of consistency with existing hydro-dynamic numerical simulations of convection (e.g., Spruit et al. 1990). The simulations reproduce with realism a large number of observables (e.g., Stein & Nordlund 1998; Asplund et al. 2000), even though they do not include magnetic fields. Could the quiet Sun have large amounts of magnetic flux and energy without modifying the convective pattern in a significant way? In other words, what are the minimum unsigned flux and energy required to alter the convective pattern? These are open questions to be addressed with realistic numerical simulations of magneto-convection.

On final comment is order. We simplify the problem of characterizing the quiet Sun magnetic field strengths using a single representative PDF. However, it is to be expected that different constituents of the quiet Sun have very different PDFs. For example, we do not distinguish between the PDFs of granules and intergranules although both numerical simulations (Cattaneo 1999; Vögler 2003) and measurements (Socas-Navarro et al. 2004; Trujillo Bueno et al. 2004) indicate a clear preference of the strong fields for the intergranules. The separation between the PDFs in granules and intergranules remains pending of future work. Similarly, the Zeeman PDF adopted in §2.1 is taken from a specific observation, and it may depend on the spatial resolution and other specificities of the particular observation. Studying such dependence remains pending too.

Thanks are due to Alexander Vögler for providing the numerical PDFs used in the work and shown in Figures 2 and 7. Thanks are also due to the referee for helpful comments. The work has been partly funded by the Spanish Ministry of Science and Technology, project AYA2004-05792, as well as by Swiss International Space Science Institute.

## APPENDIX

### THE UNBIASED PDF IS A LINEAR COMBINATION OF BIASED PDFS COMING FROM ZEEMAN AND HANLE MEASUREMENTS

The spectra used to derive magnetic field strengths from the Zeeman polarization signals have a finite spatial resolution. Therefore, two polarities often co-exist in the resolution elements, which cancels part of the polarization signals. As a result, the Zeeman measurements provide only a fraction  $f(B)$  of the quiet Sun magnetic fields with strength  $B$ . The complementary

$1 - f(B)$  is interpreted as field free. Using the symbols  $P(B)$  for the true PDF,  $\tilde{P}_Z(B)$  for the biased PDF inferred from Zeeman signals, and  $\delta(B)$  for a Dirac  $\delta$ -function,

$$\tilde{P}_Z(B) = P(B)f(B) + [1 - \langle f \rangle] \delta(B), \quad (\text{A1})$$

with  $\langle f \rangle$  the fraction of magnetized quiet Sun according to the biased Zeeman measurements,

$$\langle f \rangle = \int_0^\infty f(B)P(B)dB, \quad (\text{A2})$$

and  $\tilde{P}_Z(B)$  normalized to unity. We ignore the details of how the fraction  $f(B)$  depends on the field strength  $B$ . However, it is to be expected that the bias of the Zeeman PDF increases toward low field strengths because the polarization signals weaken with decreasing field strength (e.g. Unno 1956; Landi Degl'Innocenti & Landi Degl'Innocenti 1973). In addition, the bias  $f(B)$  should not vary with the field strength for magnetic fields stronger than a certain limit  $B_1$ . We conjecture that given a spatial resolution, the cancellation of polarization signals becomes independent  $B$  when  $B > B_1$ . One can summarize these general conditions to be satisfied by  $f(B)$  as,

$$f(B) \simeq \begin{cases} \ll f_1 & B \rightarrow 0, \\ f_1 & B > B_1. \end{cases} \quad (\text{A3})$$

Likewise, the PDF derived from Hanle signals,  $P_H(B)$ , also differs from the true PDF. The difference is parametrized by  $g(B)$ ,

$$P_H(B) = \frac{g(B)}{\langle g \rangle} P(B). \quad (\text{A4})$$

The function  $g(B)$  is also unknown, except that it has to allow  $P_H(B)$  to be a good approximation of  $P(B)$  at small field strengths. In addition, the Hanle signals are insensitive to field strengths larger than the so-called Hanle saturation  $B_2$  (see § 1). This fact allows us to assume  $g(B) \simeq 0$  for  $B > B_2$  since no information on the true PDF is provided by  $P_H(B)$ ,

$$g(B) \simeq \begin{cases} 1 & B \rightarrow 0, \\ 0 & B > B_2. \end{cases} \quad (\text{A5})$$

For the sake of convenience, we consider  $\tilde{P}_Z(B)$  without the  $\delta$ -function. After normalization, the process renders a new Zeeman PDF,

$$P_Z(B) = [\tilde{P}_Z(B) - (1 - \langle f \rangle) \delta(B)] \langle f \rangle^{-1} = \frac{f(B)}{\langle f \rangle} P(B). \quad (\text{A6})$$

In principle, one could infer the value of  $P(B)$  from both the Zeeman PDF,

$$P(B) = P_Z(B) \frac{\langle f \rangle}{f(B)}, \quad (\text{A7})$$

and the Hanle PDF,

$$P(B) = P_H(B) \frac{\langle g \rangle}{g(B)}. \quad (\text{A8})$$

In fact, any linear combination of equations (A7) and (A8) also renders the true PDF,

$$P(B) = h(B) P_Z(B) \frac{\langle f \rangle}{f(B)} + [1 - h(B)] P_H(B) \frac{\langle g \rangle}{g(B)}, \quad (\text{A9})$$

with a free weighting function  $h(B)$ . If one chooses  $h(B)$  to be,

$$h(B) = \frac{f(B)}{f_1}, \quad (\text{A10})$$

then,

$$P(B) = \frac{\langle f \rangle}{f_1} P_Z(B) + \left[1 - \frac{f(B)}{f_1}\right] \frac{\langle g \rangle}{g(B)} P_H(B), \quad (\text{A11})$$

or adding and subtracting  $\langle g \rangle P_H(B)$ ,

$$P(B) = \frac{\langle f \rangle}{f_1} P_Z(B) + \langle g \rangle P_H(B) + \left[1 - \frac{f(B)}{f_1} - g(B)\right] P(B). \quad (\text{A12})$$

The third term of this general expression is negligible for both small and large  $B$ , i.e.,

$$1 - f(B)/f_1 - g(B) \ll 1. \quad (\text{A13})$$

When  $B$  is large then  $g(B) \simeq 0$  and  $f(B) \simeq f_1$  (see equations [A3] and [A5]). The same happens for small  $B$  since  $f(B)/f_1 \ll 1$  and  $g(B) \simeq 1$  (equations [A3] and [A5]). Continuity arguments suggest that the term also vanishes for intermediate strengths, so that

$$P(B) \simeq \frac{\langle f \rangle}{f_1} P_Z(B) + \langle g \rangle P_H(B). \quad (\text{A14})$$

Using the normalization condition,

$$\int_0^\infty P(B) dB = \int_0^\infty P_Z(B) dB = \int_0^\infty P_H(B) dB = 1, \quad (\text{A15})$$

the expression (A14) can be rewritten as,

$$P(B) \simeq w P_H(B) + (1-w) P_Z(B), \quad (\text{A16})$$

with  $w = 1 - \langle f \rangle / f_1$ . Note that,

$$w < 1 - \langle f \rangle, \quad (\text{A17})$$

since  $f_1 < 1$ . Then the weight  $w$  has to be smaller than one minus the filling factor that the Zeeman signals assign to the magnetic fields of the quiet Sun (equation [A2]). This constraint is used in the main text.

In short, with very unspecific assumptions on the biases affecting the observed Zeeman and Hanle PDFs, one can approximate the true PDF as a linear combination of the observed biased Zeeman and Hanle PDFs.

### WHY UBIQUITOUS WEAK FIELDS DO NOT PRODUCE SIGNIFICANT ZEEMAN SIGNALS.

The sensitivity of the current Zeeman measurements would allow us to detect a magnetic field of one G or even smaller if it is uniform and fills completely the resolution element (e.g., Keller et al. 1994; Lites et al. 1996; Lin & Rimmele 1999; Khomenko et al. 2003). According to the arguments in the main text, most of the solar surface is occupied by magnetic fields with strengths larger than this sensitivity limit which, however, do not show up in the Zeeman measurements (c.f. the measured Zeeman PDFs in Figure 1 with the unbiased PDF in Figure 7). Actually, the Zeeman signals seem to be dominated by the polarization created by strong magnetic fields, despite the fact they only fill a small fraction of the solar surface. Signals from opposite polarities existing in the resolution element cancel out, an effect invoked to explain the difference between the real and the observed PDF (Appendix A). Why does this bias affect preferentially the weak fields? Why do the small magnetic field strength signals cancel more efficiently than those from large field strengths?

The observed bias can be understood if the size of the unresolved magnetic structures contributing to the Zeeman signals is uncorrelated with the magnetic field strength. (The typical size of a unipolar structure does not depend very much on its field strength.) Then, typically, each resolution element contains far more structures having weak fields than structures with strong fields. The cancellation is more effective when there are many structures that cancel signals, which explains the bias. This qualitative argument can be quantified as follows. A unipolar patch produces a circular polarization Stokes  $V$  signal which, to first order, scales with the field strength<sup>5</sup>. Then the Stokes  $V$  signal to be expected in a finite resolution element due to magnetic fields of strength  $B$  is

$$V = V_0 B \mu(B) [N^+(B) - N^-(B)], \quad (\text{B1})$$

with  $N^+(B)$  and  $N^-(B)$  the number of structures with positive and negative polarities in the resolution element. The symbol  $V_0$  stands for an irrelevant constant, whereas  $\mu(B)$  represents the typical value of the cosine of the magnetic field inclination with respect to the vertical direction. (We consider observations made at the disk center.) The number  $N^+(B)$  can be regarded as a random variable, in the sense that it has different values in different resolution elements. Since it is a number of counts, the random variable  $N^+(B)$  follows a Poisson distribution (e.g., Martin 1971), whose expected value and variance are identical,

$$E\{N^+(B)\} = \vee\{N^+(B)\}. \quad (\text{B2})$$

Moreover,

$$P(B) = E\{N^+(B) + N^-(B)\} (l/L)^2, \quad (\text{B3})$$

with  $L$  and  $l$  the size of the resolution element and size of one of the magnetic elements, respectively. (The factor  $[l/L]^2$  is the number of structures required to cover a resolution element.) There is no preferred polarity, consequently,

$$E\{N^-(B)\} = E\{N^+(B)\}. \quad (\text{B4})$$

Equations (B3) and (B4) lead to

$$E\{N^+(B)\} = \frac{P(B)}{2} (L/l)^2. \quad (\text{B5})$$

If the random variables  $N^+(B)$  and  $N^-(B)$  are independent, one can readily compute the mean signal and the variance to be expected due to the imperfect cancellation of the two polarities. Using equations (B1), (B2), (B4), and (B5),

$$E\{V\} = V_0 B \mu(B) [E\{N^+(B)\} - E\{N^-(B)\}] = 0, \quad (\text{B6})$$

whereas,

$$\vee\{V\} = [V_0 B \mu(B)]^2 (\vee\{N^+(B)\} + \vee\{N^-(B)\}) = [V_0 B \mu(B) L/l]^2 P(B). \quad (\text{B7})$$

The typical Stokes  $V$  signals to be expected would be of the order of standard deviation of the distribution of signals  $\sigma_V$ ,

$$\sigma_V \equiv \sqrt{\vee\{V\}} = (V_0 L/l) B \mu(B) \sqrt{P(B)}. \quad (\text{B8})$$

<sup>5</sup> The linear polarization signals scale with the square of the magnetic field strength and, therefore, the bias toward large field strengths discussed in this appendix is even more severe in linear polarization.

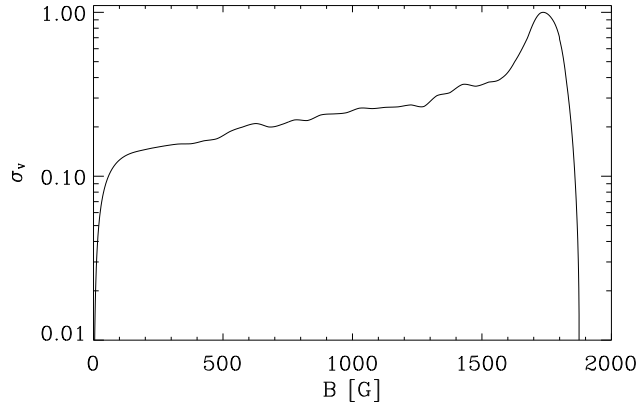


FIG. B9.— Typical Zeeman signals to be expected for each field strength  $B$ . Despite the fact that the weak fields overwhelmingly dominate the distribution of field strengths, they leave very small signals. This bias is partly due to the scaling of the Stokes  $V$  with the field strength, but it is also due to a preferential canceling of the mixed polarity weak fields. The ordinates have been scaled so that the maximum equals one.

Note that the Zeeman polarization signals due to  $B$  do not scale with their filling factor  $P(B)$  but with  $\sqrt{P(B)}$ . This scaling favors the contribution of the improbable magnetic fields, that is to say, the contribution of the large field strengths. Figure B9 shows  $\sigma_V$  normalized so that the maximum equals one. It uses the reference  $P(B)$  in Figure 7 plus the ansatz,

$$\mu(B) = \frac{1}{4} \tanh[(B - 750 \text{ G})/300 \text{ G}] + \frac{3}{4} \simeq \begin{cases} 1/2 & B < 500 \text{ G}, \\ 1 & B > 1000 \text{ G}, \end{cases} \quad (\text{B9})$$

although the latter is secondary since  $\mu(B)$  only varies from 1/2, for an isotropic distribution of magnetic field, to 1, for vertical fields. Equation (B9) parameterizes our theoretical prejudices; the distribution of inclinations should be more isotropic for weak fields (which can be easily tilted by the drag of the granulation flows) and more vertical for the strong fields (for which the buoyancy is important; see, e.g., Schüssler 1986). Figure B9 shows how the magnetic fields occupying most of the surface (say,  $B < 200 \text{ G}$ ; Figure 7) leave Stokes  $V$  signals smaller than those of the kG fields.

In short, it is not difficult to explain why the Zeeman signals tend to detect strong fields, despite the fact that they occupy a small fraction of the solar surface. It is due to the scaling of the Stokes  $V$  signals with the field strength, plus the random cancellation of the mixed polarity. The latter preferentially affects the most probable field strengths, i.e., the smallest ones.

#### REFERENCES

- Asplund, M., Nordlund, Å., Trampedach, R., Allende Prieto, C., & Stein, R. F. 2000, *A&A*, 359
- Bommier, V., Derouich, M., Landi Degl'Innocenti, E., Molodij, G., & Sahal-Bréchet, S. 2005, *A&A*, 432, 295
- Cattaneo, F. 1999, *ApJ*, 515, L39
- Domínguez Cerdeña, I. 2004, PhD thesis, Göttingen University, Göttingen
- Domínguez Cerdeña, I., Kneer, F., & Sánchez Almeida, J. 2003a, *ApJ*, 582, L55
- Domínguez Cerdeña, I., Sánchez Almeida, J., & Kneer, F. 2003b, *A&A*, 407, 741
- . 2005, *ApJ*, in preparation
- Emonet, T., & Cattaneo, F. 2001, *ApJ*, 560, L197
- Faurobert, M., Arnaud, J., Vigneau, J., & Frish, H. 2001, *A&A*, 378, 627
- Faurobert-Scholl, M. 1993, *A&A*, 268, 765
- Faurobert-Scholl, M., Feautrier, N., Machefer, F., Petrovay, K., & Spielfiedel, A. 1995, *A&A*, 298, 289
- Grossmann-Doerth, U., Keller, C. U., & Schüssler, M. 1996, *A&A*, 315, 610
- Harvey-Angle, K. L. 1993, PhD thesis, Utrecht University, Utrecht
- Howard, R., & Bhatnagar, A. 1969, *Sol. Phys.*, 10, 245
- Keller, C. U., Deubner, F.-L., Egger, U., Fleck, B., & Povel, H. P. 1994, *A&A*, 286, 626
- Khomenko, E. V., Collados, M., Solanki, S. K., Lagg, A., & Trujillo-Bueno, J. 2003, *A&A*, 408, 1115
- Khomenko, E. V., Martínez González, M. J., Collados, M., Solanki, S. K., Ruiz Cobo, B., & Beck, C. 2005, *A&A*, 436, L27
- Landi Degl'Innocenti, E. 1992, in *Solar Observations: Techniques and Interpretation*, ed. F. Sánchez, M. Collados, & M. Vázquez (Cambridge: Cambridge University Press), 71
- Landi Degl'Innocenti, E. 1998, *Nature*, 392, 256
- Landi Degl'Innocenti, E., & Landi Degl'Innocenti, M. 1973, *Sol. Phys.*, 31, 299
- Lin, H., & Rimmele, T. 1999, *ApJ*, 514, 448
- Lites, B. W. 2002, *ApJ*, 573, 431
- Lites, B. W., Leka, K. D., Skumanich, A., Martínez Pillet, V., & Shimizu, T. 1996, *ApJ*, 460, 1019
- Lites, B. W., & Socas-Navarro, H. 2004, *ApJ*, 613, 600
- Livingston, W. C., & Harvey, J. W. 1975, *BAAS*, 7, 346
- Maltby, P., Avrett, E. H., Carlsson, M., Kjeldseth-Moe, O., Kurucz, R. L., & Loeser, R. 1986, *ApJ*, 306, 284
- Manso Sainz, R., Landi Degl'Innocenti, E., & Trujillo Bueno, J. 2004, *ApJ*, 614, L89
- Martin, B. R. 1971, *Statistics for Physicists* (London: Academic Press)
- Sánchez Almeida, J. 2003, *A&A*, 411, 615
- Sánchez Almeida, J., Domínguez Cerdeña, I., & Kneer, F. 2003, *ApJ*, 597, L177
- Sánchez Almeida, J., Márquez, I., Bonet, J. A., Domínguez Cerdeña, I., & Muller, R. 2004, *ApJ*, 609, L91
- Sakurai, T. 1989, *Space Science Reviews*, 51, 11
- Sánchez Almeida, J. 1998, in *ASP Conf. Ser.*, Vol. 155, *Three-Dimensional Structure of Solar Active Regions*, ed. C. E. Alissandrakis & B. Schmieder (San Francisco: ASP), 54
- Sánchez Almeida, J. 2004, in *ASP Conf. Ser.*, Vol. 325, *The Solar-B Mission and the Forefront of Solar Physics*, ed. T. Sakurai & T. Sekii (San Francisco: ASP), 115, (astro-ph/0404053)
- Sánchez Almeida, J. 2005, *A&A*, 438, 727
- Sánchez Almeida, J., Asensio Ramos, A., Trujillo Bueno, J., & Cernicharo, J. 2001, *ApJ*, 555, 978
- Sánchez Almeida, J., Emonet, T., & Cattaneo, F. 2003, *ApJ*, 585, 536
- Sánchez Almeida, J., Landi Degl'Innocenti, E., Martínez Pillet, V., & Lites, B. W. 1996, *ApJ*, 466, 537
- Sánchez Almeida, J., & Lites, B. W. 2000, *ApJ*, 532, 1215
- Schrijver, C. J., & Title, A. M. 2003, *ApJ*, 597, L165

- Schüssler, M. 1986, in *Small Scale Magnetic Flux Concentrations in the Solar Photosphere*, ed. W. Deinzer, M. Knölker, & H. H. Voigt (Göttingen: Vandenhoeck & Ruprecht), 103
- Sigwarth, M., Balasubramaniam, K. S., Knölker, M., & Schmidt, W. 1999, *A&A*, 349, 941
- Smithson, R. C. 1975, *BAAS*, 7, 346
- Socas-Navarro, H., Martínez Pillet, V., & Lites, B. W. 2004, *ApJ*, 611, 1139
- Socas-Navarro, H., & Sánchez Almeida, J. 2002, *ApJ*, 565, 1323
- . 2003, *ApJ*, 593, 581
- Spruit, H. C. 1976, *Sol. Phys.*, 50, 269
- . 1981a, *A&A*, 98, 155
- Spruit, H. C. 1981b, in *The Sun as a Star*, ed. S. Jordan, NASA SP-450 (Washington: NASA), 385
- Spruit, H. C., Nordlund, Å., & Title, A. M. 1990, *ARA&A*, 28, 263
- Stein, R. F., & Nordlund, Å. 1998, *ApJ*, 499, 914
- Stein, R. F., & Nordlund, Å. 2002, in *IAU Colloquium 188*, ed. H. Sawaya-Lacoste, ESA SP-505 (Noordwijk: ESA Publications Division), 83
- Stenflo, J. O. 1982, *Sol. Phys.*, 80, 209
- . 1994, *Solar Magnetic Fields*, ASSL 189 (Dordrecht: Kluwer)
- Stenflo, J. O., Bianda, M., Keller, C. U., & Solanki, S. K. 1997, *A&A*, 322, 985
- Stenflo, J. O., & Lindegren, L. 1977, *A&A*, 59, 367
- Title, A. M., & Berger, T. E. 1996, *ApJ*, 463, 797
- Trujillo Bueno, J. 2001, in *ASP Conf. Ser.*, Vol. 236, *Advanced Solar Polarimetry – Theory, Observation, and Instrumentation*, ed. M. Sigwarth (San Francisco: ASP), 161
- Trujillo Bueno, J., Shchukina, N. G., & Asensio Ramos, A. 2004, *Nature*, 430, 326
- Unno, W. 1956, *PASJ*, 8, 108
- . 1959, *ApJ*, 129, 375
- Vögler, A., Shelyag, S., Schüssler, M., Cattaneo, F., Emonet, T., & Linde, T. 2005, *A&A*, 429, 335
- Vögler, A. 2003, PhD thesis, Göttingen University, Göttingen
- Wang, J., Wang, H., Tang, F., Lee, J. W., & Zirin, H. 1995, *Sol. Phys.*, 160, 277
- Yi, Z., Jensen, E., & Engvold, O. 1993, in *ASP Conf. Ser.*, Vol. 46, *The Magnetic and Velocity Fields of Solar Active Regions*, ed. H. Zirin, G. Ai, & H. Wang, San Francisco, 232